Analysis of the Interaction Between a Layered Spherical Human Head Model and a Finite-Length Dipole

Konstantina S. Nikita, *Senior Member, IEEE*, Georgios S. Stamatakos, Nikolaos K. Uzunoglu, *Senior Member, IEEE*, and Aggelos Karafotias

***Abstract*—The coupling between a finite-length dipole antenna and a three-layer lossy dielectric sphere, representing a simplified model of the human head, is analyzed theoretically in this paper. The proposed technique is based on the theory of Green's functions in conjunction with the method of auxiliary sources (MAS). The Green's function of the three-layer sphere can be calculated as the response of this object to the excitation generated by an elementary dipole of unit dipole moment. The MAS is then applied to model the dipole antenna by distributing a set of auxiliary current sources on a virtual surface lying inside the antenna physical surface. By imposing appropriate boundary conditions at a finite number of points on the real surface of the antenna, the unknown auxiliary sources coefficients can be calculated and, hence, the electric field at any point in space can be easily obtained. Numerical results concerning the specific absorption rate inside the head, the total power absorbed by the head, the input impedance, and the radiation pattern of the antenna are presented for homogeneous and layered head models exposed to the near-field radiation of half-wavelength dipoles at 900 and 1710 MHz. The developed method can serve as a reliable platform for the assessment of purely numerical electromagnetic methods. The method can also provide an efficient tool for accurate testing and comparison of different antenna designs since generalizations required to treat more complex antenna configurations are straightforward.**

***Index Terms*—Biological effects of electromagnetic radiation, dipole antennas, electromagnetic coupling, Green's function, mobile communication.**

I. Introduction

THE ever expanding use of hand-held tranceivers operating in close proximity to the human head has raised public concern about potential health effects and compliance with standards. On the other hand, the effect of the head on the performance of the mobile phone antenna and the need to improve antenna design have further motivated research efforts to study the interactions between mobile communications handsets and the human body.

Several calculation techniques, such as finite-difference time-domain (FDTD) algorithms [1]–[6], method of moments (MoM) [7], multiple multipole method (MMP) [8], and analytical methods [9]–[11] have been used by many researchers in order to evaluate the interaction between human head and mobile phone antennas. These analyses range from simple models of the human head, such as a homogeneous sphere to heterogeneous anatomically correct models based on magnetic resonance imaging.

Furthermore, considerable efforts have been devoted on an international level to ensure both the validity and applicability of numerical methods in terms of computing time and memory demands. Therefore, basic canonical problems have been proposed for the comparison of different numerical treatments [12]. In an associated study performed within the framework of the COST 244 Project, it has been shown that significant discrepancies can be observed in the results obtained by different groups nominally using a very similar numerical method, even for well-defined canonical cases. These discrepancies are related with specific implementation details of the numerical method adopted, as it is also pointed out in [13], where the effect of antenna numerical representation and absorbing boundary conditions in FDTD modeling of canonical exposure problems is studied. In this context, the treatment of simple models is necessary for computer code checking and allows the comparison of different purely numerical techniques, while analytical and semianalytical methods provide indispensable tools for independent validation and accuracy assessment of numerical techniques.

Much work to approach the problem of interaction of electromagnetic radiation with parts of the human body in an analytical way has been performed [9]–[11], [14]–[22]. Simplified models of the head, most frequently homogeneous or multilayered concentric [11], [15], [18], [21] or eccentric [10] spheres have been used. The choice of these geometries was essentially due to the necessity of characterizing a structure resembling a human head and having at the same time a closed form of the wave equation. In the above works, either a plane wave [9], [10] or a localized source exposure, such as a dipole or a loop [10], [11], [14], [21] is considered. Furthermore, a predefined distribution for the incident waveform or the current along the antenna is assumed [9]–[11], [14]–[18], [21] and the effect of the head model on the source current distribution is not taken into account. However, recent efforts, based on numerical methods, have been focused on the study of the interaction between the antenna and biological object [1]–[3], [23]–[25], especially for characterizing the antenna performance.

In this paper, a semianalytical technique is presented based on the use of the dyadic Green's function theory [21], [26] and the method of auxiliary sources (MAS) [27], [28], to model the interaction between a layered spherical model of the human head

Manuscript received November 12, 1999; revised May 3, 2000. This work was supported under the EC SMT Programme, Cellular Phone Standard Project.

The authors are with the Department of Electrical and Computer Engineering, National Technical University of Athens, 157 80 Athens, Greece.

Publisher Item Identifier S 0018-9480(00)09691-5.

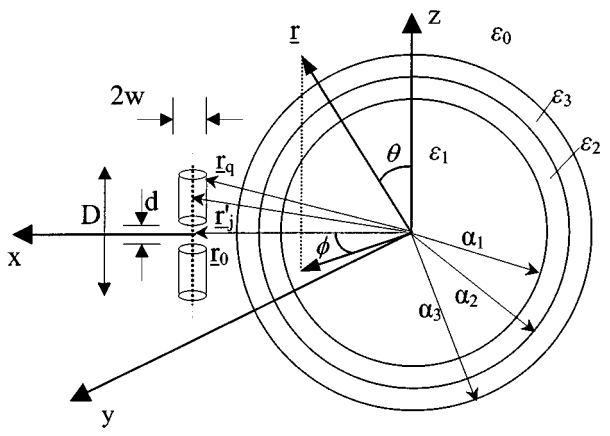

Fig. 1. Three-layer lossy dielectric sphere exposed to the near-field radiation of a finite-length dipole.

and a finite-length dipole antenna, placed at its close proximity. The developed technique takes into account the modification of the current along the dipole due to the presence of the head. The MAS is a very efficient numerical technique, which is able to provide accurate solutions of scattering problems, with relatively low computational demands. According to the MAS, a set of auxiliary current sources with unknown coefficients are distributed on virtual surfaces usually conforming to the real surfaces of the examined scattering structures. By imposing the appropriate boundary conditions at a finite number of points on the physical surfaces of the scatterers, the unknown coefficients of the auxiliary sources are determined. In the problem examined in this paper, the dipole antenna is modeled by considering a set of auxiliary sources (e.g., elementary dipoles) distributed along its axis since the diameter of the antenna is usually substantially less than the radiation wavelength (e.g., at 900 and 1800 MHz).

This paper is organized as follows. In Section II, the formulation and analysis for the problem of interaction between a three-layer lossy dielectric sphere and a dipole antenna are presented, followed by the necessary checks for the validation of the developed method in Section III. In Section IV, both a homogeneous and a three-layer head model exposed to the radiation of a half-wavelength dipole are considered, and numerical results are presented at 900 and 1710 MHz for the specific absorption rate (SAR) distribution, the maximum SAR values averaged over 1 and 10 g of tissue, the antenna input impedance, and radiation pattern.

II. Mathematical Formulation and Analysis

The head is modeled by a three-layer sphere with radii α_1, α_2, and α_3, as shown in Fig. 1. The three layers can be used to simulate different biological media, such as skin, bone, and brain tissues. The dielectric properties of the layers are denoted with the corresponding complex permittivities $\varepsilon_1, \varepsilon_2, \varepsilon_3$. The magnetic properties of the layers are defined as $\mu_1 = \mu_2 = \mu_3 = \mu_0$. Free space is assumed for the exterior of the sphere with wavenumber $k_0 = \omega\sqrt{\varepsilon_0, \mu_0}$, where ω is the radian frequency and ε_0 and μ_0 are the free-space permittivity and permeability, respectively.

The dipole antenna is modeled by two metallic cylinders, $2w$ in diameter, separated by the feeding gap of length d. The length of the entire antenna (including the feeding gap) is D and the position vector of its center is $\underline{r}_0 = x_0\hat{x}$. Although the axis of the antenna can generally have any orientation, for the sake of simplicity, it is assumed parallel to the z-axis of the coordinate's system, as shown in Fig. 1. The time dependence of the field quantities is assumed to be $\exp(-j\omega t)$ and it is suppressed throughout the analysis. In order to solve this boundary value problem, a Green's function technique in conjunction with the MAS is adopted.

A. Dyadic Green's Function of the Layered Sphere

First, the Green's function of the three-layer sphere is determined as the response of this object to the excitation generated by an elementary dipole of unit dipole moment, external to the sphere [21]. To determine the Green's function of the three-layer lossy dielectric sphere, a method based on the superposition principle is employed [21]. According to this method, the unknown dyadic Green's function in each region $i = 1, 2, 3, 4$ of space is properly expanded as an infinite sum of spherical waves satisfying the appropriate vector wave equation. Then, the boundary conditions on the interfaces $r = \alpha_1, \alpha_2, \alpha_3$ determine the unknown expansion coefficients [21], [26]. Thus, considering the finiteness of the field at $r = 0$, the following expressions hold for the electric-type Green's function inside the layered sphere:

$$\overline{G}_1(\underline{r},\underline{r}') = \sum_{n=1}^{+\infty}\sum_{m=-n}^{n}\Big[\underline{m}_{mn}^{(1)}(\underline{r},k_1)\underline{a}_{mn}(\underline{r}') + \underline{n}_{mn}^{(1)}(\underline{r},k_1)\underline{A}_{mn}(\underline{r}')\Big], \qquad r \le a_1 \tag{1}$$

$$\overline{G}_2(\underline{r},\underline{r}') = \sum_{n=1}^{+\infty}\sum_{m=-n}^{n}\Big[(\underline{m}_{mn}^{(1)}(\underline{r},k_2)\underline{b}_{mn}^{(1)}(\underline{r}') + \underline{n}_{mn}^{(1)}(\underline{r},k_2)\underline{B}_{mn}^{(1)}(\underline{r}')) + (\underline{m}_{mn}^{(2)}(\underline{r},k_2)\underline{b}_{mn}^{(2)}(\underline{r}') + \underline{n}_{mn}^{(2)}(\underline{r},k_2)\underline{B}_{mn}^{(2)}(\underline{r}')\Big], \quad a_1 \le r \le a_2 \tag{2}$$

$$\overline{G}_3(\underline{r},\underline{r}') = \sum_{n=1}^{+\infty}\sum_{m=-n}^{n}\Big[(\underline{m}_{mn}^{(1)}(\underline{r},k_3)\underline{c}_{mn}^{(1)}(\underline{r}') + \underline{n}_{mn}^{(1)}(\underline{r},k_3)\underline{C}_{mn}^{(1)}(\underline{r}')) + (\underline{m}_{mn}^{(2)}(\underline{r},k_3)\underline{c}_{mn}^{(2)}(\underline{r}') + \underline{n}_{mn}^{(2)}(\underline{r},k_3)\underline{C}_{mn}^{(2)}(\underline{r}')\Big], \quad a_2 \le r \le a_3 \tag{3}$$

where $k_i = k_0\sqrt{\varepsilon_i}$, $\underline{\alpha}_{mn}(\underline{r}'), \underline{A}_{mn}(\underline{r}'), \ldots, \underline{C}_{mn}^{(2)}(\underline{r}')$ are unknown coefficients to be determined and $\underline{m}_{mn}^{(j)}(\underline{r},k_i), \underline{n}_{mn}^{(j)}(\underline{r},k_i)$, $i = 1, 2, 3$; $j = 1, 2$ are the well-known spherical wave functions [26].

In the region outside the three-layer sphere, the electric field $\overline{G}_4(\underline{r},\underline{r}')$ is due to the primary excitation $\overline{G}_0(\underline{r},\underline{r}')$ from the unit source located at $\underline{r}'$ and the field $\overline{G}_s(\underline{r},\underline{r}')$ scattered from the spherical object

$$\overline{G}_4(\underline{r},\underline{r}') = \overline{G}_0(\underline{r},\underline{r}') + \overline{G}_s(\underline{r},\underline{r}'). \tag{4}$$

In (4), $\overline{\underline{G}}_0(\underline{r},\underline{r}')$ is the well-known free-space dyadic Green's function, and is expressed in terms of spherical waves as [26]

$$\overline{\underline{G}}_0(\underline{r},\underline{r}') = \sum_{n=1}^{+\infty}\sum_{m=-n}^{n}(jk_0)\frac{(-1)^m(2n+1)}{4\pi n(n+1)} \times \begin{cases} \Big[\underline{m}_{mn}^{(1)}(\underline{r},k_0)\underline{m}_{-mn}^{(3)}(\underline{r}',k_0) \\ \quad +\underline{n}_{mn}^{(1)}(\underline{r},k_0)\underline{n}_{-mn}^{(3)}(\underline{r}',k_0)\Big], & r<r' \\ \Big[\underline{m}_{mn}^{(3)}(\underline{r},k_0)\underline{m}_{-mn}^{(1)}(\underline{r}',k_0) \\ \quad +\underline{n}_{mn}^{(3)}(\underline{r},k_0)\underline{n}_{-mn}^{(1)}(\underline{r}',k_0)\Big], & r>r'. \end{cases} \tag{5}$$

The scattered field $\overline{\underline{G}}_s(\underline{r},\underline{r}')$ of (4) should satisfy the radiation conditions. Therefore, it should be expanded as [26]

$$\overline{\underline{G}}_s(\underline{r},\underline{r}') = \sum_{n=1}^{+\infty}\sum_{m=-n}^{n}\Big[\underline{m}_{mn}^{(3)}(\underline{r},k_0)\underline{d}_{mn}(\underline{r}') + \underline{n}_{mn}^{(3)}(\underline{r},k_0)\underline{D}_{mn}(\underline{r}')\Big], \qquad r\geq a_3. \tag{6}$$

The boundary conditions for the continuity of the tangential electric and magnetic field components are then imposed on the interfaces $r=\alpha_1,\ \alpha_2,\ \alpha_3$

$$\hat{\underline{r}}\times\overline{\underline{G}}_i(\underline{r},\underline{r}') = \hat{\underline{r}}\times\overline{\underline{G}}_{i+1}(\underline{r},\underline{r}'), \qquad r=\alpha_i;\ i=1,2,3 \tag{7}$$

$$\hat{\underline{r}}\times\Big[\nabla\times\overline{\underline{G}}_i(\underline{r},\underline{r}')\Big] = \hat{\underline{r}}\times\Big[\nabla\times\overline{\underline{G}}_{i+1}(\underline{r},\underline{r}')\Big], \qquad r=a_i;\ i=1,2,3 \tag{8}$$

where $\hat{r}$ denotes the unit vector along the radial direction of the coordinates system illustrated in Fig. 1. By making use of the orthogonality properties of the spherical wave functions [26], two independent 6×6 linear sets of equations are obtained for the unknown expansion coefficients. These two independent sets can be solved analytically for the coefficients $\underline{\alpha}_{mn},\underline{b}_{mn}^{(\ell)},\underline{c}_{mn}^{(\ell)}$ and $\underline{A}_{mn},\underline{B}_{mn}^{(\ell)},\underline{C}_{mn}^{(\ell)}$ $(\ell=1,2)$, respectively. The end result for the Green's function in each region $i=1,\ 2,\ 3,\ 4$ can then be written in the form

$$\overline{\underline{G}}_i(\underline{r},\underline{r}') = \sum_{n=1}^{+\infty}\sum_{m=-n}^{n}\frac{jk_0(-1)^m(2n+1)}{4\pi n(n+1)} \cdot\Bigg\{\Big[Q_n^{(i,1)}\underline{m}_{mn}^{(1)}(\underline{r},k_i) + Q_n^{(i,2)}\underline{m}_{mn}^{(\ell)}(\underline{r},k_i)\Big]\underline{m}_{-mn}^{(3)}(\underline{r}',k_0) + \Big[R_n^{(i,1)}\underline{n}_{mn}^{(1)}(\underline{r},k_i) + R_n^{(i,2)}\underline{n}_{mn}^{(\ell)}(\underline{r},k_i)\Big]\underline{n}_{-mn}^{(3)}(\underline{r}',k_0)\Bigg\} \tag{9}$$

where $\ell=2$ for $i=1,\ 2,\ 3/\ell=3$ for $i=4$.

The detailed expressions for the scalar coefficients $Q_n^{(i,k)},R_n^{(i,k)}i=1,\ 2,\ 3,\ 4;\ k=1,\ 2$ appearing in (9) are given in the Appendix.

B. MAS

The dipole antenna of the examined structure (Fig. 1) is modeled by applying the MAS. The MAS is a general method able to model both dielectric and conducting objects. The principal idea of MAS is based on the concept of distributing a set of auxiliary current sources with unknown coefficients on virtual surfaces usually conforming to the real surfaces of the examined scattering structures [27], [28]. Thus, auxiliary sources are distributed on auxiliary surfaces lying inside and outside each scatterer, to describe the external and internal excited fields, respectively. For conducting objects, only one (internal) surface is required to describe the external field, while for dielectric media, two surfaces are required to describe both the external and internal fields. Using as auxiliary sources, fundamental solutions of the Helmholtz equation with unknown weighting coefficients and imposing the boundary conditions for the electric- and magnetic-field components at a finite number of points lying on the real conducting or dielectric surfaces, the unknown weighting coefficients of the auxiliary sources can then be determined and the fields at any point of interest can then be easily obtained.

For the problem of the dipole antenna treated in this paper, since its diameter is usually substantially less than the radiation wavelength, a number J of auxiliary sources (elementary dipoles) are distributed along the axis of the dipole antenna, with corresponding position vectors $\underline{r}_j = x_0\hat{x}+z_j\hat{z}$, where $-D/2\leq z_j\leq D/2$ and $j=1,\ldots,J$. The electric field at a point $\underline{r}$ lying in any region $i=1,\ 2,\ 3,\ 4$ can be expressed as

$$\underline{E}_i(\underline{r}) = j\omega\mu_0\sum_{j=1}^{J}\overline{\underline{G}}_i\Big(\underline{r},\underline{r}_j'\Big)\underline{L}_j'\Big(\underline{r}_j'\Big) \tag{10}$$

where $\overline{\underline{G}}_i(\underline{r},\underline{r}_j')$ is the dyadic Green's function in the corresponding region and $\underline{L}_j'(\underline{r}_j')$ is the dipole moment of each elementary dipole–auxiliary source positioned at $\underline{r}_j'$.

Since the elementary dipoles are aligned parallel to the z-axis, their dipole moments can be further expressed as

$$\underline{L}_j'(\underline{r}_j') = \hat{z}p_j', \qquad j=1,\ldots,J$$

where p_j' denotes the constant moment magnitude of the jth elementary dipole.

According to the MAS, appropriate boundary conditions should be applied at a number of points on the surface of the antenna in order to calculate the unknown coefficients $\underline{L}_j'(\underline{r}_j')$. Thus, the boundary conditions for the tangential electric-field component vanishing on the conducting surface of the dipole—with the exception of the feeding gap—are imposed at a finite number of (collocation) points lying along a line on the surface of the dipole, with corresponding position vectors $\underline{r}_q=(x_0-w)\hat{x}+z_q\hat{z}$, with $-D/2\leq z_q\leq D/2$

$$\hat{z}\cdot\underline{E}_4(\underline{r}_q) = \begin{cases} 0, & \text{if } \left|\frac{d}{2}\right|<|z_q|<\left|\frac{D}{2}\right| \\ \frac{V_0}{d}, & \text{if } |z_q|\leq\left|\frac{d}{2}\right| \end{cases}, \qquad q=1,\ldots,J \tag{11}$$

TABLE I
MASS DENSITY (ρ), REAL PART (ε'), AND IMAGINARY PART (ε'') OF THE DIELECTRIC PERMITTIVITY OF TISSUES USED IN THE SIMULATIONS

	900MHz		1710MHz	
Tissue	ε'	ε''	ε'	ε''
Skin (ρ=1100 kg/m^3)	39.5	14.0	38.2	9.9
Bone (cortical/skull) (ρ=1200 kg/m^3)	12.5	3.4	12.0	3.0
Brain (grey matter) (ρ=1050 kg/m^3)	56.8	22.0	51.8	16.0

where $\underline{E}_4$ is calculated using (10) and V_0 is the voltage imposed at the feeding gap.

By enforcing (11), a $J \times J$ system of linear equations is obtained, which is solved for the unknown dipole moment coefficients p'_j. Once these coefficients are computed, the electric field can then be calculated at any point inside and outside the spherical head model, according to closed form (10), with a remarkably low computational cost. From the electric field, two derivative quantities of practical interest, the SAR and the scattering amplitude in the radiation zone, can be obtained.

From the above description, it can be observed that, in the specific case of the dipole treated in this paper, the application of the MAS is similar with the treatment of thin wires by the traditional MoM [29].

It is important to note that the above-presented method is quite general as far as the radiating source is concerned. Thus, in the case of more complex antenna configurations, such as helical antennas, the same treatment applies if adequate geometrical description of the real surface points, on which the boundary conditions are imposed, is provided.

III. VALIDATION OF THE METHOD

In order to check the developed numerical code, several trials have been performed. The convergence and stability of the proposed technique have been checked in detail and validation results are presented in this section for the case of a homogeneous spherical head model $2\alpha_3 = 20$ cm in diameter, consisting of brain. The spherical head model is exposed to the radiation of a dipole operating at 1710 MHz, with its center placed at the point $\underline{r}_0 = 10.625\hat{x}$ (cm) (see Fig. 1), and having the following geometric characteristics: length $D = \lambda/2$ (λ is the free-space wavelength), feeding gap $d = 0.25$ cm, conductor diameter $2w = 0.25$ cm. The real part (ε') and the imaginary part (ε'') of the brain complex dielectric permittivity used in the calculations have been defined according to literature data [30] and are shown in Table I.

The prediction of the electric field at any point in space involves the computation of a double sum with respect to the integers n and m referring to the spherical wave vectors used to express the fields inside the layers of the sphere and in the air region [see (9)]. The infinite sum with respect to n is convergent and, therefore, it can be truncated to a finite one. The number of terms required for the infinite sum to converge depends on the size of the spherical object, its electrical characteristics, and the distance of the elementary dipole from the outer surface of the sphere. For the specific cases treated in this paper, it has been observed that truncation of the infinite sum with respect to the order n of the spherical wave vectors as high as $N = 45$ ensures convergence of the obtained solution at any point. However, a significantly lower number of terms ($N = 8$) is sufficient to assure convergence of the solution at far-field points. Convergence patterns are presented in Fig. 2 for the current induced along the dipole for the specific case examined in this section.

The far-field predictions of the Green's function code have been compared with those of the Mie theory for the case of a homogeneous sphere irradiated by a plane wave at 1710 MHz. The plane-wave irradiation of the dielectric sphere has been simulated by considering a $\hat{z}$ oriented elementary dipole (see Fig. 1) placed at the far-field point $\underline{r}_0 = -100\hat{x}$ m and selecting its moment to produce a plane wave with unit electric-field amplitude at the plane $x = 0$. Detailed comparison of the scattered field values at different points lying at a distance of 15 m from the center of the sphere obtained by the Green's function approach and Mie theory [31] has shown an excellent agreement, as presented in Table II.

The convergence and stability of the obtained solution have also been examined by increasing the number of auxiliary sources used to model the dipole. Convergence patterns in terms of the current induced on the dipole are presented in Fig. 2. A total number of $J = 359$ auxiliary sources has been found sufficient to assure convergence of the solution. Furthermore, the continuity of the tangential fields at the $r = a_1$, $r = a_2$, and $r = a_3$ interface planes between different layers has been checked and verified numerically, while the validity of the boundary conditions on the surface of the dipole has also been checked.

Energy conservation has been checked by comparing the input power computed at the feeding gap, to the sum of the power absorbed by the head, and the power radiated in the antenna far field, and has shown an excellent agreement (difference of the order of 1%).

Finally, comparison of the results obtained using the proposed semianalytical technique with results obtained using the FDTD method has shown a difference of the order of 2% in the prediction of both local peak SAR value and input impedance real part [13], when an infinitely thin wire approximation and a hard sinusoidal source are used for the FDTD dipole antenna representation.

IV. NUMERICAL RESULTS AND DISCUSSION

The developed method has been used to study the interaction between dipole antennas and two spherical models of the head; a homogeneous sphere consisting of brain tissue and a three-layer sphere consisting of skin, skull, and brain. Both head models have a diameter of $2a_3 = 20$ cm, while the thicknesses of the skin and skull layers for the layered head model are as-

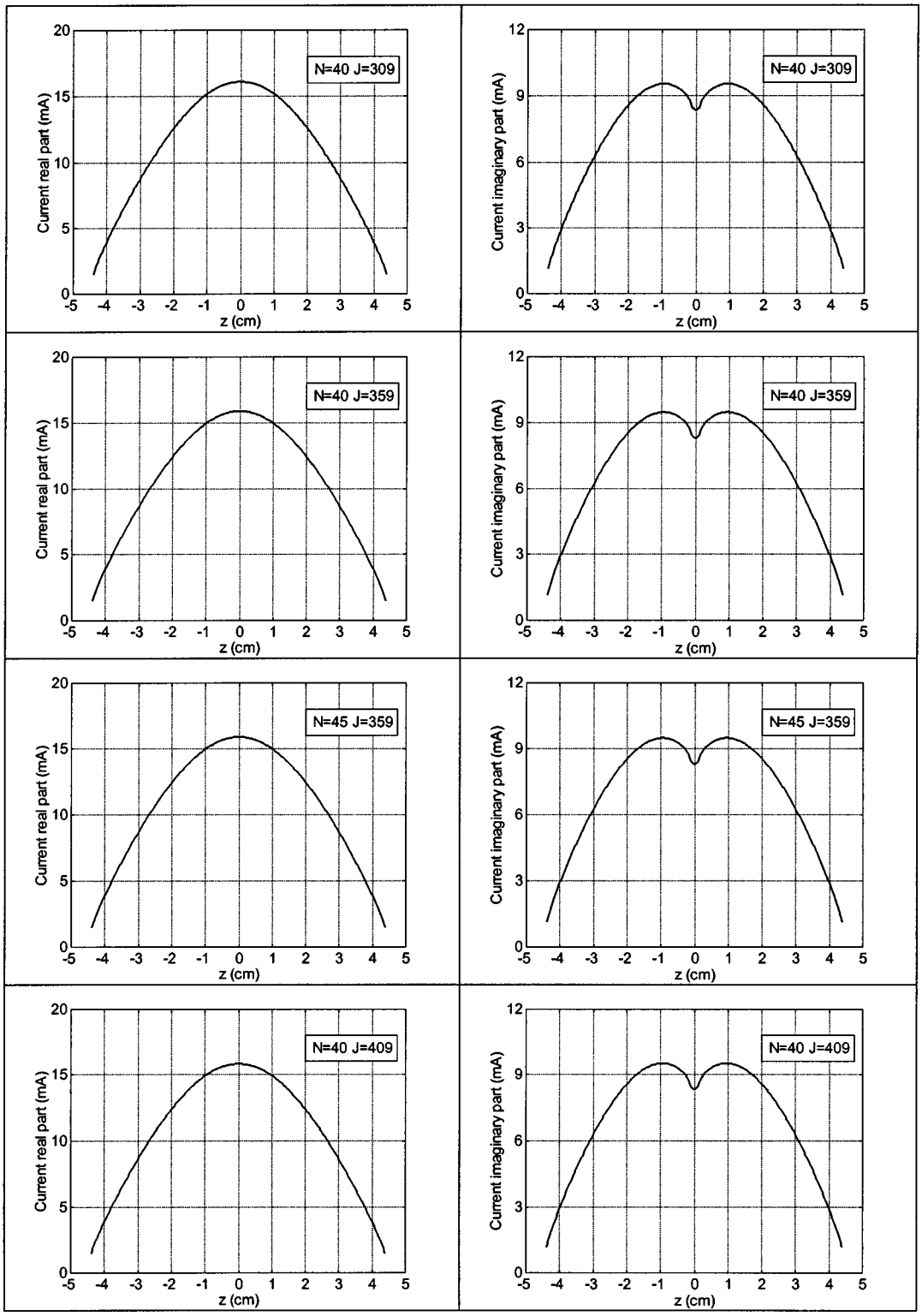

Fig. 2. Convergence patterns for the current induced along a half-wavelength dipole at 1710 MHz by increasing the number J of auxiliary sources used to model the dipole and the number N of spherical waves used for the expansion of the fields. The voltage imposed at the feeding gap is 1 V.

sumed to be $a_3 - a_2 = 0.5$ cm, $a_2 - a_1 = 0.5$ cm, respectively. Calculations have been performed for half-wavelength dipoles, centered at the point $\underline{r}_0 = 10.625\hat{x}$ cm, with geometrical characteristics identical to those described in Section III at both 900 and 1710 MHz. Table I summarizes the mass density (ρ), real part (ε'), and imaginary part (ε'') of the complex dielectric permittivity allocated to the tissues used for the calculations at 900 and 1710 MHz [30].

The developed semianalytical technique has been used to predict the value of peak SAR within the head models, SAR profiles along x-axis, SAR distributions at the $y = 0$ cm plane, total power absorbed by the head, antenna input impedance

TABLE II
COMPARISON OF THE GREEN'S FUNCTION TECHNIQUE SCATTERED FIELD PREDICTIONS WITH MIE THEORY FOR A HOMOGENEOUS SPHERICAL HEAD MODEL AT 1710 MHz

OBSERVATION POINT		SCATTERED FIELD MAGNITUDE ($\times 10^{-2}$ V/m)	
θ(°)	ϕ(°)	GREEN	MIE
45	180	0.1867	0.1859
45	270	0.2715	0.2708
90	0	1.4723	1.4717
90	180	0.3074	0.3075
90	270	0.3185	0.3177
180	0	0.2823	0.2821

TABLE III
HOMOGENEOUS AND LAYERED SPHERICAL HEAD MODELS EXPOSED TO THE RADIATION OF A HALF-WAVELENGTH DIPOLE AT 900 AND 1710 MHz: PEAK SAR VALUES, ABSORBED POWER, DIPOLE INPUT IMPEDANCE. THE ANTENNA INPUT POWER IS 1 W

	Homogeneous sphere		Three-layer sphere	
	900 MHz	1710 MHz	900 MHz	1710 MHz
Peak local SAR (W/kg)	39.4	92.95	29.3	72.3
Peak 1g-SAR (W/kg)	17.5	34.31	10.37	29.3
Peak 10g-SAR (W/kg)	10.07	19.54	7.12	13.5
Power absorbed by the head (W)	0.77	0.76	0.75	0.83
Input impedance at the feeding gap (Ω)	(53.5,14.0)	(49.2, 25.9)	(67.0,24.1)	(66.2,16.3)

and antenna radiation patterns at two planes ($\theta = 90°$ and $\phi = 0°$).

For all the graphs presenting the results of the computations, the steady-state radiated power from the antenna is 1 W (i.e., the power radiated in the far field plus the power dissipated in the head).

A. SAR Computations and Absorbed Power

The electric field and local SAR values at different points inside the sphere have been predicted. Furthermore, mass-averaged SAR values have been computed since the basic restrictions applied for Mobile Terminal Equipment compliance testing are defined in terms of average SAR values over a tissue mass of 1 [32], [33] or 10 g [34]–[36]. The reference 1- or 10-g tissue mass is defined in the safety standards as a cube according to ANSI–IEEE and CENELEC [32], [33], [35], [36] or as "any 10 g of contiguous tissue," according to ICNIRP [34]. In this paper, the SAR averaged over 1 or 10 g of tissue is computed by the equation

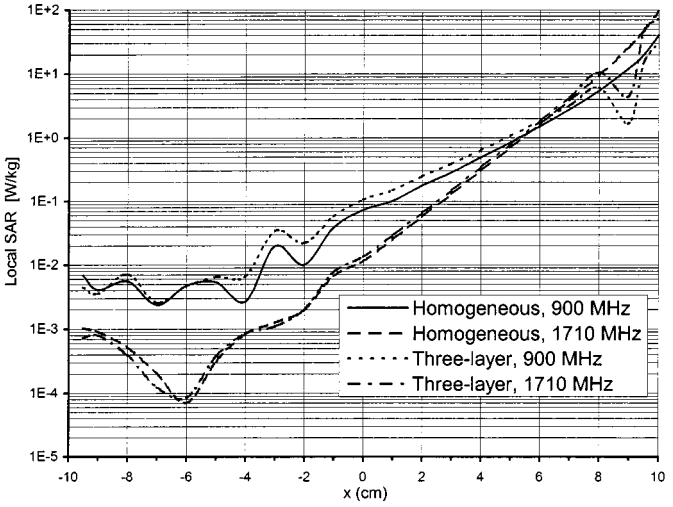

(a)

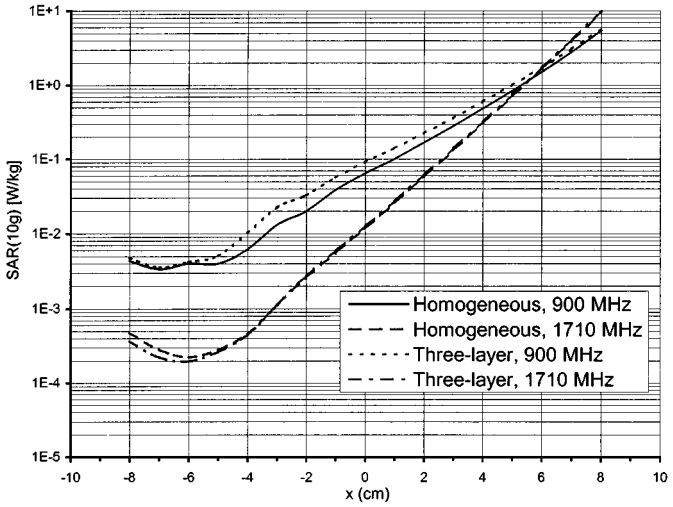

(b)

Fig. 3. Variation of SAR along x-axis. The antenna input power is 1 W. (a) Local SAR. (b) SAR averaged over 10 g.

$$\mathrm{SAR}_M(\underline{r}) = \frac{\iiint_{V=a^3} \mathrm{SAR}(\underline{r}')\rho(\underline{r}')\, d\underline{r}'}{\iiint_{V=a^3} \rho(\underline{r}')\, d\underline{r}'} \tag{12}$$

where the denominator represents the mass contained in a cubic cell of size a, centered at point $\underline{r}$, which should be equal to the reference mass M. In general, for the case of a layered sphere, the size of the cube centered at the point of interest containing the reference mass M is not *a priori* known and has to be determined by applying an iterative procedure. Of course, for the homogeneous sphere case, the cube size containing the reference mass can be easily determined in a single step by considering the constant mass density of the sphere. As long as the cube size containing the reference tissue mass has been determined,

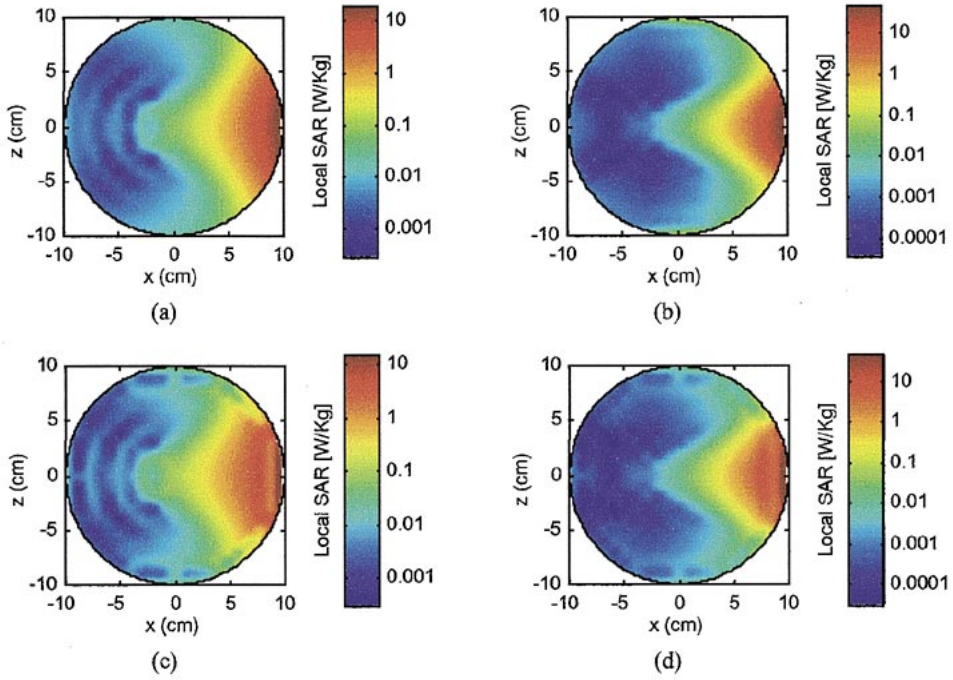

Fig. 4. Local SAR distributions on the $y = 0$-plane. The antenna input power is 1 W. (a) homogeneous spherical head model (dipole at 900 MHz). (b) Homogeneous spherical head model (dipole at 1710 MHz). (c) Three-layer spherical head model (dipole at 900 MHz). (d) Three-layer spherical head model (dipole at 1710 MHz).

the integration limits encountered in (12) can be calculated and the pertaining integrations can be performed. Since the subvolumes to consider for evaluating the average SARs at superficial points are not clearly defined in the CENELEC [35], [36], ICNIRP [34] and ANSI–IEEE [32] safety guidelines, in this paper, the averaging procedure has been performed only for a cube full of tissue. Of course, the most crucial problem remains the evaluation of the average SARs at superficial points, which are of great importance, since high local SAR values are observed at these points.

The maximum values of the local SAR, SAR averaged over 1 g, and SAR averaged over 10 g of tissue have been computed and are shown in Table III for the homogeneous and layered head phantoms at 900 and 1710 MHz, for 1 W of radiated power.

As expected, the maximum local SAR value is dependent on the frequency. The maximum local SARs at 1710 MHz are larger than those at 900 MHz (for the same radiated power) and this difference is due to the difference in the penetration depth. In general, homogeneous sphere models give increased values for local and averaged SARs compared to layered ones.

The SAR average over 1 g of tissue is 1.5–2 times greater than the average over 10 g of tissue. The averaging mass of 10 g is small enough not to disguise any strong local heating, but is large enough not to place undue weight on the localized heating of small structures. However, in performing SAR averaging over 10 g, important high local SAR regions lying very close to the head surface have not been taken into account because it is not possible to obtain cubes with a mass of 10 g, containing such regions, as it has already been explained.

Furthermore, the penetration curves, which are the SAR variation from "one ear to the other" (along x-axis in Fig. 1) of the spherical head models, have been computed and are shown in Fig. 3 for both local SAR values and SAR values, as averaged over 10 g of tissue.

Fig. 4 shows the distributions of the local SAR, at the xz-plane ($y = 0$ cm) for the different cases. The results can be summarized as follows. The absorbed power distribution in the head models is strongly inhomogeneous. The region with high absorption values in all head models is small and close to the feedpoint of the dipole. The power absorption at 1710 MHz occurs more superficially than at 900 MHz. In the high-frequency case, the antennas are physically smaller. Accordingly, the regions of high SAR values are more concentrated. Moreover, no significant differences are observed between the SAR distributions inside the homogeneous sphere and those in the layered model.

Finally, the power absorbed by the spherical head models for 1-W radiated power has been computed and is presented in Table III. Typically, a 75%–83% of the dipole radiated power is absorbed by the head models. The total power of $P_i = 1$ W radiated from the source, calculated at the feeding gap, has been imposed by using the equation $P_i = \mathrm{Re}\{V_0 \cdot I_0^*\}$, where V_0 and I_0 denote the voltage and current at the center of the feeding gap.

B. Antenna Performance

The input impedance of the dipole antenna has been calculated as $Z_i = V_0/I_0$. In Table III, the real and imaginary parts of the antenna input impedance for the examined canonical cases are presented. Due to the small source-head distance and the resulting strong electromagnetic coupling effect, the input impedance shifts far from resonance, exhibiting a significant imaginary part.

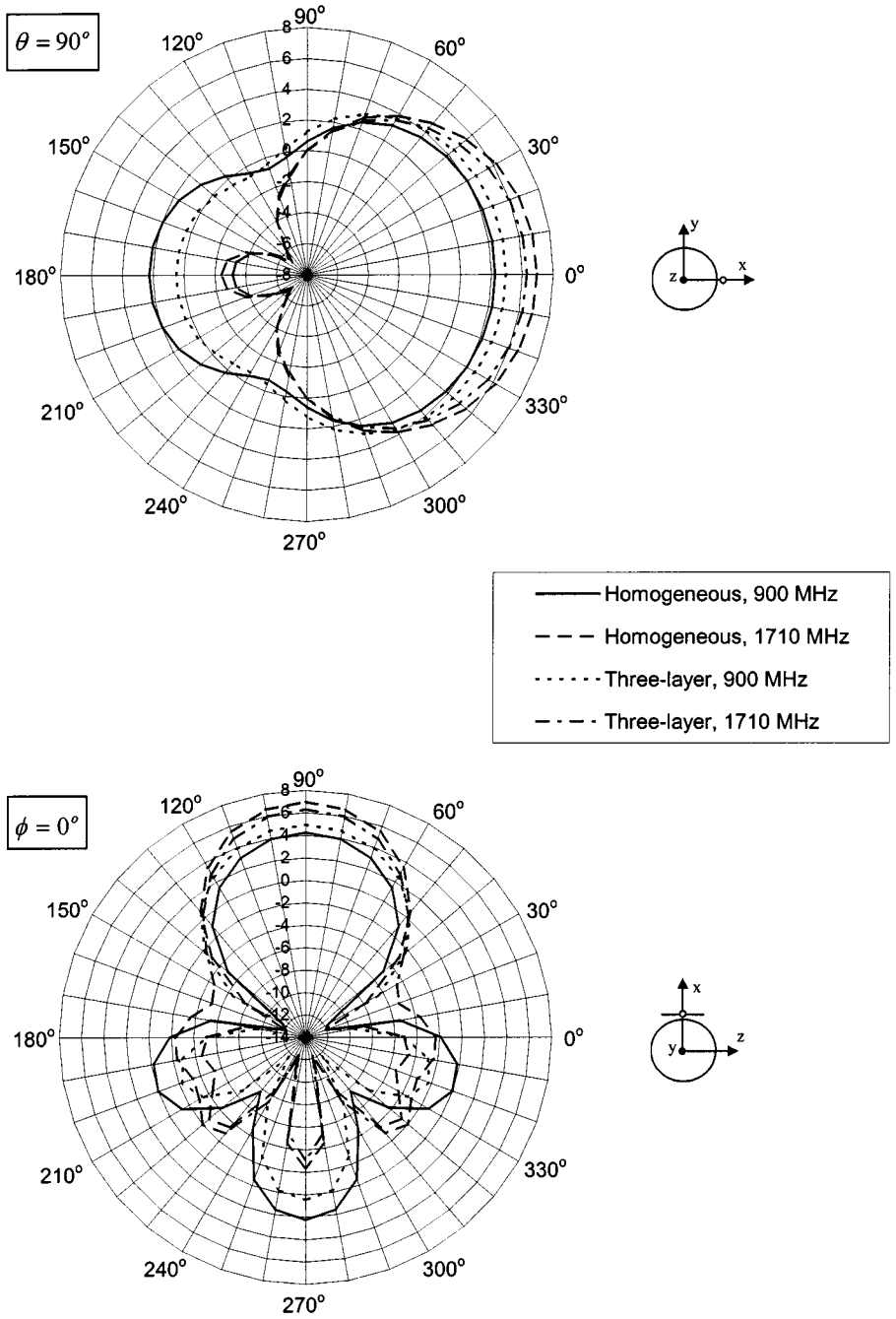

Fig. 5. Radiation pattern (dBi) of a half-wavelength dipole radiating close to a homogeneous or a three-layer spherical head model at 900 and 1710 MHz.

Furthermore, the influence of the head model on the radiation characteristics of the dipole has been determined. In computing the radiation pattern, the reference system attached to the center of the spherical head model has been used (Fig. 1). In Fig. 5, results for the far-field radiation pattern of the dipole are shown for the homogeneous and layered spherical head models at 900 and 1710 MHz at both xy-planes ($\theta = 90°$) and xz-planes ($\phi = 0°$). As expected, the spherical head models strongly disturb the symmetry of the radiation pattern. By absorption and reflection of the power incident on the head, the far-field radiation pattern in the direction of the head decreases, especially at the higher frequency, as was expected. The decrease in the direction where the head is located is slightly larger for the layered sphere structure than for the homogeneous one.

V. Conclusions

In this paper, a semianalytical technique has been presented for the study of interaction between a layered spherical model of the human head and a finite-length dipole antenna placed at its close proximity. The proposed method is based on the combination of the Green's function methodology with the MAS. Extensive validation checks of the developed technique have been performed. Numerical results have been presented for the

cases of homogeneous and three-layer models of the head exposed to the radiation of half-wavelength dipole antennas at 900 and 1710 MHz. A number of physical quantities describing both the electromagnetic power deposition within the spherical head models and degradation of the telecommunication efficiency have been evaluated. The application presented, apart from constituting a worst-case approximation for the radiation hazards, seems to be a reliable and computationally efficient platform for the assessment of purely numerical electromagnetic methods. Furthermore, since generalizations of the proposed method to treat more complex antenna configurations are straightforward, the method can provide an efficient and accurate tool for testing and comparing different antenna designs.

APPENDIX

The scalar coefficients $Q_n^{(i,k)}$, $R_n^{(i,k)} i = 1, 2, 3, 4; k = 1, 2$ appearing in (9) are given as follows:

$$\begin{aligned} Q_n^{(4,1)} &= 1 \\ R^{(4,1)} &= 1 \end{aligned} \tag{A1}$$

$$\begin{aligned} Q_n^{(3,1)} &= W_n^{(1)} \\ R_n^{(3,1)} &= W_n^{(2)} \end{aligned} \tag{A2}$$

$$\begin{aligned} Q_n^{(2,1)} &= W_n^{(3)} Q_n^{(3,1)} \\ R_n^{(2,1)} &= W_n^{(4)} R_n^{(3,1)} \end{aligned} \tag{A3}$$

$$\begin{aligned} Q_n^{(1,1)} &= W_n^{(5)} Q_n^{(2,1)} \\ R_n^{(1,1)} &= W_n^{(6)} R_n^{(2,1)} \end{aligned} \tag{A4}$$

$$\begin{aligned} Q_n^{(4,2)} &= P_n^{(1)} \\ R_n^{(4,2)} &= P_n^{(2)} \end{aligned} \tag{A5}$$

$$\begin{aligned} Q_n^{(3,2)} &= S_n^{(1)} Q_n^{(3,1)} \\ R_n^{(3,2)} &= S_n^{(2)} R_n^{(3,1)} \end{aligned} \tag{A6}$$

$$\begin{aligned} Q_n^{(2,2)} &= T_n^{(1)} Q_n^{(2,1)} \\ R_n^{(2,2)} &= T_n^{(2)} R_n^{(2,1)} \end{aligned} \tag{A7}$$

$$\begin{aligned} Q_n^{(1,2)} &= 0 \\ R_n^{(1,2)} &= 0. \end{aligned} \tag{A8}$$

The quantities appearing in (A2)–(A7) are obtained by the equations

$$W_n^{(1)} = \frac{j_n(k_0\alpha_3) - P_n^{(1)} h_n(k_0\alpha_3)}{j_n(k_3\alpha_3) - S_n^{(1)} y_n(k_3\alpha_3)} \tag{A9}$$

$$W_n^{(2)} = \varepsilon_3 \frac{j_n^d(k_0\alpha_3) - P_n^{(2)} h_n^d(k_0\alpha_3)}{j_n^d(k_3\alpha_3) - S_n^{(2)} y_n^d(k_3\alpha_3)} \tag{A10}$$

$$W_n^{(3)} = \frac{j_n(k_3\alpha_2) - S_n^{(1)} y_n(k_3\alpha_2)}{j_n(k_2\alpha_2) - T_n^{(1)} y_n(k_2\alpha_2)} \tag{A11}$$

$$W_n^{(4)} = \frac{\varepsilon_2}{\varepsilon_3} \frac{j_n^d(k_3\alpha_2) - S_n^{(2)} y_n^d(k_3\alpha_2)}{j_n^d(k_2\alpha_2) - T_n^{(2)} y_n^d(k_2\alpha_2)} \tag{A12}$$

$$W_n^{(5)} = \frac{j_n(k_2\alpha_1) - T_n^{(1)} y_n(k_2\alpha_1)}{j_n(k_1\alpha_1)} \tag{A13}$$

$$W_n^{(6)} = \frac{\varepsilon_1}{\varepsilon_2} \frac{j_n^d(k_2\alpha_1) - T_n^{(2)} y_n^d(k_2\alpha_1)}{j_n^d(k_1\alpha_1)} \tag{A14}$$

where j_n, y_n, h_n are the spherical Bessel, Neuman, and Hankel functions, respectively, $z_n^d(x) = (d[xz_n(x)]/dx)$, with z_n being either of the j_n, y_n, h_n functions

$$\begin{aligned} T_n^{(1)} &= \frac{U_{jj}^{(1)}}{U_{jy}^{(i)}} \\ T_n^{(2)} &= \frac{V_{jj}^{(1)}}{V_{jy}^{(i)}} \end{aligned} \tag{A15}$$

$$\begin{aligned} S_n^{(1)} &= \frac{U_{jj}^{(2)} + T_n^{(1)} U_{yj}^{(2)}}{U_{jy}^{(2)} + T_n^{(1)} U_{yy}^{(2)}} \\ S_n^{(2)} &= \frac{V_{jj}^{(2)} + T_n^{(2)} V_{yj}^{(2)}}{V_{jy}^{(2)} + T_n^{(2)} V_{yy}^{(2)}} \end{aligned} \tag{A16}$$

$$\begin{aligned} P_n^{(1)} &= \frac{U_{jj}^{(3)} + S_n^{(1)} U_{yj}^{(3)}}{U_{jh}^{(3)} + S_n^{(1)} U_{yh}^{(3)}} \\ P_n^{(2)} &= \frac{V_{jj}^{(3)} + S_n^{(2)} V_{yh}^{(3)}}{V_{jh}^{(3)} + S_n^{(2)} V_{yh}^{(3)}}. \end{aligned} \tag{A17}$$

The quantities in (A15)–(A17) are given as

$$U_{\kappa\lambda}^{(i)} = \kappa_n(k_0\varepsilon_i\alpha_i)\lambda_n^d(k_0\varepsilon_{i+1}\alpha_i) - \kappa_n^d(k_0\varepsilon_i\alpha_i)\lambda_n(k_0\varepsilon_{i+1}\alpha_i) \tag{A18}$$

$$\begin{aligned} V_{\kappa\lambda}^{(i)} = {} & [k_0\varepsilon_i\alpha_i]^2 \kappa_n(k_0\varepsilon_i\alpha_i)\lambda_n^d(k_0\varepsilon_{i+1}\alpha_i) \\ & - [k_0\varepsilon_{i+1}\alpha_i]^2 \kappa_n^d(k_0\varepsilon_i\alpha_i)\lambda_n(k_0\varepsilon_{i+1}\alpha_i) \end{aligned} \tag{A19}$$

where $\kappa_n(x)$, $\lambda_n(x)$ are either of the spherical Bessel, Neumann, or Hankel functions.

REFERENCES

[1] M. Okoniewski and M. A. Stuchly, "A study of the handset antenna and human body interaction," *IEEE Trans. Microwave Theory Tech.*, vol. 44, pp. 1855–1864, Oct. 1996.

[2] O. P. Gandhi and J.-Y. Chen, "Electromagnetic absorption in the human head from experimental 6-GHz handheld transceivers," *IEEE Trans. Electromag. Compat.*, vol. 37, pp. 547–558, Apr. 1995.

[3] M. A. Jensen and Y. Rahmat-Samii, "EM interaction of handset antennas and a human in personal communications," *Proc. IEEE*, vol. 83, pp. 7–17, Jan. 1995.
[4] P. J. Dimbylow and O. P. Gandhi, "Finite-difference time-domain calculations of SAR in a realistic heterogeneous model of the head for plane-wave exposure from 600 MHz to 3 GHz," *Phys. Med. Biol.*, vol. 36, no. 8, pp. 1075–1089, 1991.
[5] P. J. Riu and K. R. Foster, "Heating of tissue by near-field exposure to a dipole: A model analysis," *IEEE Trans. Biomed. Eng.*, vol. 46, pp. 911–917, Aug. 1999.
[6] P. J. Dimbylow and S. M. Mann, "SAR calculations in an anatomically realistic model of the head for mobile communication transceivers at 900 MHz and 1.8 GHz," *Phys. Med. Biol.*, vol. 39, no. 9, pp. 1537–1553, 1994.
[7] H.-R. Chuang, "Human operator coupling effects on radiation characteristics of a portable communications dipole antenna," *IEEE Trans. Antennas Propagat.*, vol. 42, pp. 556–560, Apr. 1994.
[8] N. Kuster, "Multiple multipole method applied to an exposure safety study," *J. Appl. Comput. Electromag. Soc.*, vol. 7, pp. 43–60, 1992.
[9] A. R. Shapiro, R. F. Lutomirski, and H. T. Yura, "Induced fields and heating within a cranial structure irradiated by an electromagnetic plane wave," *IEEE Trans. Microwave Theory Tech.*, vol. MTT-19, pp. 187–196, Feb. 1971.
[10] N. C. Skaropoulos, M. P. Ioannidou, and D. P. Chrissoulidis, "Induced EM field in a layered eccentric spheres model of the head: Plane-wave and localized source exposure," *IEEE Trans. Microwave Theory Tech.*, vol. 44, pp. 1963–1973, Oct. 1996.
[11] G. Cerri, R. De Leo, and G. Rosellini, "Evaluation of electromagnetic power deposition in a spherical multilayer head in the near field of a linear antenna," *Wireless Networks*, vol. 3, pp. 499–510, 1997.
[12] G. D'Inzeo, "Proposal for numerical canonical models in mobile communications," in *Proc. COST 244 Meeting*, D. Simunic, Ed., Rome, Italy, Nov. 1994, pp. 17–19.
[13] K. S. Nikita, N. K. Uzunoglu, P. Bernardi, M. Cavagnaro, S. Pisa, E. Piuzzi, G. I. Krikelas, and J. N. Sahalos, "A study of uncertainties in modeling the handset antenna and human head interaction using the FDTD method," in *Proc. IEEE MTT-S Int. Microwave Symp.*, Boston, MA, June 11–16, 2000.
[14] J. R. Wait, "On the electromagnetic response of a conducting sphere to a dipole field," *Geophys.*, vol. XXV, no. 3, pp. 649–658, June 1960.
[15] H. N. Kriticos and H. P. Schwan, "Hot spots generated in conducting spheres by electromagnetic waves and biological implications," *IEEE Trans. Biomed. Eng.*, vol. BME-19, pp. 53–58, Jan. 1972.
[16] W. T. Joines and R. J. Spiegel, "Resonance absorption of microwaves by the human skull," *IEEE Trans. Biomed. Eng.*, vol. BME-21, pp. 46–48, Jan. 1974.
[17] C. M. Weil, "Absorption characteristics of multilayered sphere models exposed to UHF/microwave radiation," *IEEE Trans. Biomed. Eng.*, vol. BME-22, pp. 468–476, Nov. 1975.
[18] H. N. Kriticos and H. P. Schwan, "Formation of hot spots in multilayered spheres," *IEEE Trans. Biomed. Eng.*, vol. BME-23, pp. 168–172, Mar. 1976.
[19] M. F. Iskander, P. W. Barber, C. H. Durney, and H. Massoudi, "Irradiation of prolate spheroidal models of humans in the near field of a short electric dipole," *IEEE Trans. Microwave Theory Tech.*, vol. MTT-28, pp. 801–807, July 1980.
[20] N. K. Uzunoglu and E. A. Angelikas, "Field distributions in a three-layer prolate spheroidal human body model for a loop antenna irradiation," *IEEE Trans. Antennas Propagat.*, vol. AP-35, pp. 1180–1185, Oct. 1987.
[21] P. G. Cottis and N. K. Uzunoglu, "Focusing properties of dipole arrays placed near a multilayer lossy sphere," *J. Electromag. Waves Applicat.*, vol. 4, pp. 431–440, 1990.
[22] L. Li, P. Kooi, M. S. Leong, and T. S. Yeo, "Electromagnetic dyadic Green's function in spherically multilayered media," *IEEE Trans. Microwave Theory Tech.*, vol. 42, pp. 2302–2309, Dec. 1994.
[23] H.-R. Chuang, "Human operator coupling effects on radiation characteristics of a portable communications dipole antenna," *IEEE Trans. Antennas Propagat.*, vol. 42, pp. 556–560, Apr. 1994.
[24] J. Toftgard, S. N. Hornsleth, and J. B. Andersen, "Effects on portable antennas of the presence of a person," *IEEE Trans. Antennas Propagat.*, vol. 41, pp. 739–746, June 1993.
[25] H. Y. Chen and H. H. Wang, "Current and SAR induced in a human head model by electromagnetic fields irradiated from a cellular phone," *IEEE Trans. Microwave Theory Tech.*, vol. 42, pp. 2249–2254, Dec. 1994.
[26] P. M. Morse and H. Feshbach, *Methods of Theoretical Physics, Part II*. New York: McGraw-Hill, 1953, ch. 13.
[27] V. Kupradze, *Method of Integral Equations in the Theory of Diffraction*. Moscow, Russia, 1935.
[28] R. Zaridze, G. Bit-Babik, K. Tavzarashvili, N. K. Uzunoglu, and D. Economou, "The method of auxiliary sources (MAS)—Solution of propagation, diffraction and inverse problems using MAS," in *Applied Computational Electromagnetics: State of the Art and Future Trends*, N. K. Uzunoglu, K. S. Nikita, and D. I. Kaklamani, Eds. Berlin, Germany: Springer-Verlag, 2000, pp. 33–45.
[29] R. F. Harrington, "Matrix methods for field problems," *Proc. IEEE*, vol. 55, pp. 136–149, Feb. 1967.
[30] C. Gabriel, S. Gabriel, and E. Corthout, "The dielectric properties of biological tissues," *Med. Phys.*, vol. 41, pp. 2231–2293, 1996.
[31] A. Ishimaru, *Wave Propagation and Scattering in Random Media*. New York: Academic, 1978, vol. 1, pp. 27–30.
[32] *IEEE Standard for Safety Levels with Respect to Human Exposure to Radio Frequency Electromagnetic Fields, 3 kHz to 300 GHz*, IEEE Standard C95.1-1991, Sept. 1991.
[33] "Additional information for evaluating compliance of mobile and portable devices with FCC limits for human exposure to radiofrequency emissions," Federal Commun. Commission, Washington, DC, OET Bulletin 65—Supp. C, Dec. 1997.
[34] International Commission on Non-Ionising Radiation Protection, "Guidelines for limiting exposure to time-varying electric, magnetic and electromagnetic fields (up 300 GHz)," *Health Phys.*, vol. 56, 1998.
[35] *Human Exposure to Electromagnetic Fields High-Frequency: 10 kHz—300 GHz*, CENELEC, ENV 50 166-2, European Prestandard ENV 50166-2, Jan. 1995.
[36] "Considerations for human exposure to electromagnetic fields from mobile telecommunication equipment (MTE) in the frequency range 30 MHz–6 GHz," CENELEC, Brussels, Belgium, prES 59 005, Dec. 1997.

Konstatina S. Nikita (M'96–SM'00) received the Diploma degree in electrical engineering and the Ph.D. degree from the National Technical University of Athens, Athens, Greece, in 1986 and 1990, respectively, and the M.D. degree from the Medical School, University of Athens, Athens, Greece, in 1993.

Since 1990, she has been a Researcher at the Institute of Communication and Computer Systems, National Technical University of Athens. In 1996, she joined the Department of Electrical and Computer Engineering, National Technical University of Athens, where she is currently an Assistant Professor. Her current research interests include applications of electromagnetic waves in medicine, electromagnetic scattering, diffraction tomography, medical imaging and image processing, and nonlinear optimization algorithms and applications. She has been the Technical Manager of a number of European and National Research and Development projects in the field of biomedical engineering.

Dr. Nikita is a member of the Technical Chamber of Greece, the Athens Medical Association, and the Hellenic Society of Biomedical Engineering.

Georgios S. Stamatakos received the Diploma degree in electrical engineering from the National Technical University of Athens, Athens, Greece, in 1987, the M.Sc. degree in bioengineering from the University of Strathclyde, Glasgow, Scotland, in 1988, and the Ph.D. degree in physics from the National Technical University of Athens, Athens, Greece, in 1997.

From 1989 to 1990, he was with the Hellenic Army General Staff, Medical Corps Directorate. He is currently a Research Assistant Professor in the Department of Electrical and Computer Engineering, Institute of Communications and Computer Systems (ICCS), National Technical University of Athens. His research interests include electromagnetic scattering, bioelectromagnetics, biooptics, oncological simulations, and radiotherapy optimization. He has authored over 30 papers in international conferences, journals, and books.

Nikolaos K. Uzunoglu (M'82–SM'97) was born in Constantinopole, in 1951. He received the B.Sc. degree in electronics from the Technical University of Istanbul, Istanbul, Turkey, in 1973, the M.Sc. and Ph.D. degrees from the University of Essex, Essex, U.K., in 1974 and 1976, respectively, and the D.Sc. degree from the National Technical University of Athens, Athens, Greece, in 1981.

From 1977 to 1984, he was a Research Scientist in the Office of Research and Technology of the Hellenic Navy. In 1984, he became an Associate Professor at the National Technical University of Athens, Department of Electrical Engineering and, in 1987, he became a Professor. In 1986, he was elected Vice-Chairman of the Department of Electrical Engineering, National Technical University of Athens and, in 1988, he became Chairman of the same department. He was reelected as Chairman in 1990 and 1992 twice. In 1991, he became Director of the Institute of Communication and Computer Systems, an independent research establishment associated with the National Technical University of Athens, and served in this position until 1999. He has authored or co–authored over 120 papers in refereed international journals, and has authored three books in Greek on microwaves, fiber-optic telecommunications, and radar systems. His research interests include electromagnetic scattering, propagation of electromagnetic waves, fiber-optic telecommunications, and high-speed circuits operating at gigabit/second rates. Since 1988 he has been the national representative of Greece to the COST, Technical Telecommunications Committee, and has actively participating in several COST telecommunications projects. Further, he has been Project Manger of several RACE, ESPRIT, ACTS and National Research and Development Projects in the fields of telecommunications and biomedical engineering applications.

Dr. Uzunoglu was the recipient of the 1981 International G. Marconi Award in Telecommunications. In 1994, he was elected as an Honorary Professor of the State Engineering University of Armenia. He was awarded the honorary Ph.D. diploma from the Universities of Bucharest, Cluj-Napoca, and Orade. In 1998, he was elected a Foreign Member of the National Academy of Sciences of Armenia.

Aggelos Karafotias was born in Athens, Greece, in 1972. He received the Diploma degree in electrical engineering from the National Technical University of Athens (NTUA), Athens, Greece, in 1997, and is currently working toward the Ph.D. degree in electrical and computer engineering at the NTUA.

His research interests include antennas theory and techniques, electromagnetic-wave propagation, and bioelectromagnetics.